



OPEN ACCESS

EDITED BY

Wujing Cao,
Chinese Academy of Sciences (CAS), China

REVIEWED BY

Jianfeng Li,
Beijing University of Technology, China
Jiaxin Wang,
Hebei University of Technology, China

*CORRESPONDENCE

Jianye Niu,
✉ jyniu@ysu.edu.cn
Bo Cheng,
✉ Barrycb@163.com

RECEIVED 08 November 2023

ACCEPTED 20 December 2023

PUBLISHED 08 January 2024

CITATION

Tian J, Wang H, Lu H, Yang Y, Li L, Niu J and Cheng B (2024), Force/position-based velocity control strategy for the lower limb rehabilitation robot during active training: design and validation.

Front. Bioeng. Biotechnol. 11:1335071.

doi: 10.3389/fbioe.2023.1335071

COPYRIGHT

© 2024 Tian, Wang, Lu, Yang, Li, Niu and Cheng. This is an open-access article distributed under the terms of the [Creative Commons Attribution License \(CC BY\)](https://creativecommons.org/licenses/by/4.0/). The use, distribution or reproduction in other forums is permitted, provided the original author(s) and the copyright owner(s) are credited and that the original publication in this journal is cited, in accordance with accepted academic practice. No use, distribution or reproduction is permitted which does not comply with these terms.

Force/position-based velocity control strategy for the lower limb rehabilitation robot during active training: design and validation

Junjie Tian^{1,2}, Hongbo Wang^{1,2,3}, Hao Lu³, Yang Yang^{1,2}, Lianqing Li^{1,2}, Jianye Niu^{1,2*} and Bo Cheng^{4*}

¹Hebei Provincial Key Laboratory of Parallel Robot and Mechatronic System, Yanshan University, Qinhuangdao, China, ²School of Mechanical Engineering, Yanshan University, Qinhuangdao, China, ³Academy for Engineering and Technology, Fudan University, Shanghai, China, ⁴Qinhuangdao Hospital of Traditional Chinese Medicine, Qinhuangdao, China

Aiming at the shortcomings of most existing control strategies for lower limb rehabilitation robots that are difficult to guarantee trajectory tracking effect and active participation of the patient, this paper proposes a force/position-based velocity control (FPVC) strategy for the hybrid end-effector lower limb rehabilitation robot (HE-LRR) during active training. The configuration of HE-LRR is described and the inverse Jacobian analysis is carried out. Then, the FPVC strategy design is introduced in detail, including normal velocity planning and tangential velocity planning. The experimental platform for the HE-LRR system is presented. A series of experiments are conducted to validate the FPVC strategy's performance, including trajectory measurement experiments, force and velocity measurement experiments, and active participation experiments. Experimental studies show that the end effector possesses good following performance with the reference trajectory and the desired velocity, and the active participation of subjects can be adjusted by the control strategy parameters. The experiments have verified the rationality of the FPVC strategy, which can meet the requirements of trajectory tracking effect and active participation, indicating its good application prospects in the patient's robot-assisted active training.

KEYWORDS

active training, rehabilitation robot, trajectory tracking, velocity control, active participation

1 Introduction

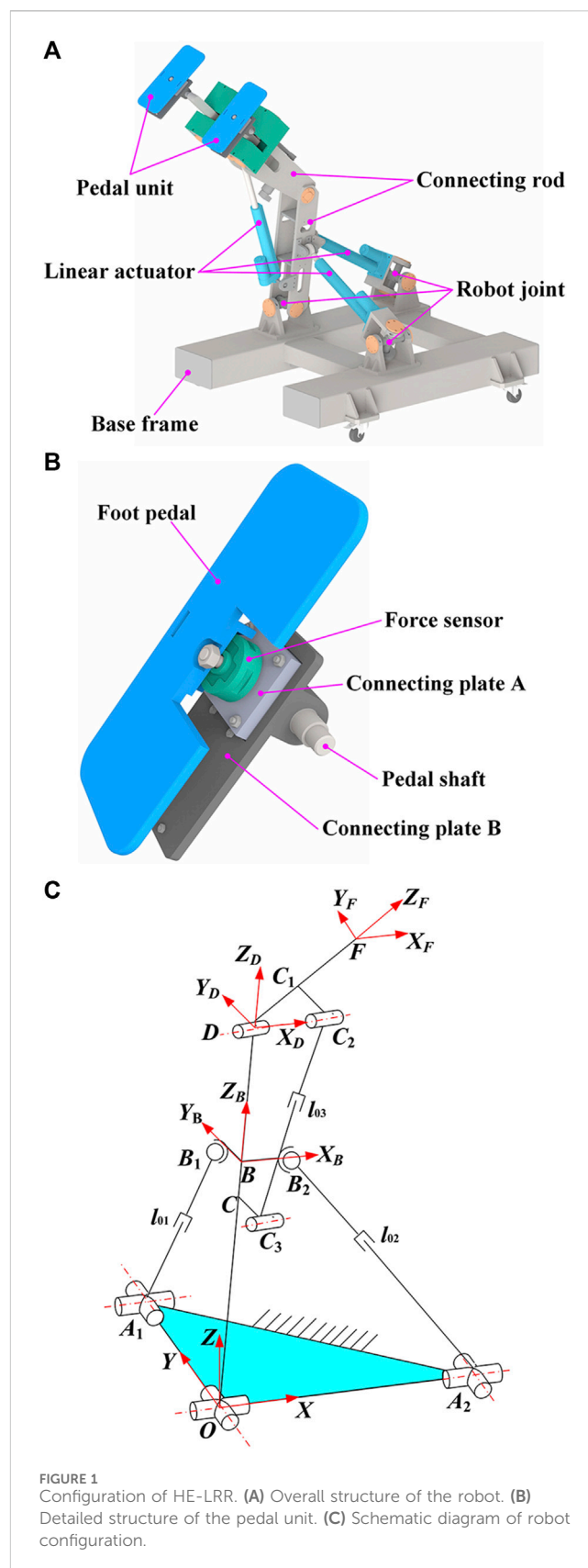
Stroke is a cerebrovascular disease that seriously endangers human health (Langhorne et al., 2011; Singh et al., 2018). Its high incidence rate and high disability rate have brought heavy burdens to individuals, families and society (Feigin et al., 2009). Epidemiological investigation shows that motor dysfunction is the leading cause of disability after stroke (Zhang et al., 2016; Dulyan et al., 2022). In recent years, many studies have been dedicated to developing rehabilitation robot systems to assist stroke patients in limb rehabilitation training, and a series of research achievements have been made (Krebs et al., 2007; Zhou et al., 2021; Cao et al., 2023).

According to patients' degree of active participation, training methods are mainly divided into two types: passive training and active training (Shi et al., 2019). The robot guides the patient's limbs along the required reference trajectory in passive training. It aims to prevent

muscle atrophy through repetitive movement (Wu et al., 2022). Passive training is suitable for improving proprioceptive sensitivity around limb joints in the early rehabilitation stage (Chiyohara et al., 2020). In active training, patients are required to complete corresponding tasks within a certain period based on verbal or visual instructions (Sun et al., 2023). Clinical research shows that the patient's active participation is conducive to motor-related cortical activation and limb rehabilitation (Zheng et al., 2021). The control strategies involved in active training are primarily based on bioelectrical signals and force/torque signals (Zhang et al., 2017).

Two active control strategies utilizing sEMG signals are available for rehabilitation robots: continuous control and triggered control (Meng et al., 2015; Cao et al., 2022). With the continuous control, sEMG signals are used to recognize the limb motion intention, and torque assistance based on this intention is provided for generating the desired motion (Lu et al., 2019). Xie et al. have combined sEMG signals with interaction force to optimize trajectory planning for the rehabilitation robot and planned different periodic trajectories (Xie et al., 2016). Khoshdel et al. developed a neural impedance control strategy to estimate the exerted force using sEMG signals for a single-DOF rehabilitation robot (Khoshdel et al., 2018). Shi et al. proposed a model for predicting the continuous motion of lower limbs for rehabilitation robots (Shi et al., 2020). Their study examined the influence of different muscle types on joint angles as well as the robustness of their prediction model. With the triggered control, the robot begins to provide the assistance when the sEMG signals reach a certain threshold (Artz, 2015). Using the support vector machine classification model, Meng et al. developed a control strategy capable of predicting limb motion intention and triggering robot assistance based on sEMG signals (Meng et al., 2014). Ma et al. used sEMG signals to predict the angles of the hip and knee joints. When the predicted angle values reached the set thresholds, the lower limb rehabilitation robot was triggered to complete the corresponding gait (Ma et al., 2019). An sEMG-based trigger was proposed by Kawamoto et al. for the HAL rehabilitation robot. By providing the patient with motion support, HAL could move the joints in accordance with the movement intention and improve the lower limb's joint mobility (Kawamoto et al., 2010). Nevertheless, bioelectrical signals used for active control are susceptible to interference and consume considerable time. Implementation and interpretation of this approach are highly dependent on the individual (Taffese, 2017).

Compared with bioelectrical signals, force/torque signals have the advantages of stable performance (Lotti et al., 2022). The active training control strategies based on force/torque information mainly include the impedance control and the hybrid force/position control strategies (Tsoi et al., 2009). The impedance control aims to synchronously adjust motion and force by establishing an appropriate interaction relationship (Zhou et al., 2021). Huo et al. developed an impedance modulation method for the exoskeleton robot, which can provide balance assistance during the switch between sitting and standing (Huo et al., 2022). Mokhtari et al. proposed a hybrid optimal sliding mode impedance control method and compared the performance with that of the traditional sliding mode controller in the lower limb exoskeleton system (Mokhtari et al., 2021). Tran et al. designed a fuzzy rule-based impedance control strategy that can adjust the impedance coefficients between the robot and the lower limb under various walking speeds (Tran et al., 2016). The hybrid position/force controller is intended for both position and force trajectory tracking



(Navvabi and Markazi, 2019). Bernhardt et al. proposed a hybrid control strategy for the rehabilitation robot Lokomat. In the swing phase, the rehabilitation robot was controlled by force so the patient

TABLE 1 Parameter symbols and descriptions of the robot configuration.

| Symbol | Description |
|----------|----------------------------------------------------------------------------------------|
| l_1 | Length of OD |
| l_2 | Length of DF |
| l_{01} | Length of A_1B_1 |
| l_{02} | Length of A_2B_2 |
| l_{03} | Length of C_2C_3 |
| a_1 | Length of OA_1 |
| a_2 | Length of OA_2 |
| b_1 | Length of BB_1 |
| b_2 | Length of BB_2 |
| a_3 | Length of CC_3 |
| b_3 | Length of C_1C_2 |
| l_{OB} | Length of OB |
| m_1 | Length of CD |
| m_2 | Length of C_1D |
| α | The angle of $\{D-X_D Y_D Z_D\}$ relative to $\{O-XYZ\}$ around the X -axis |
| β | The angle of $\{D-X_D Y_D Z_D\}$ relative to $\{O-XYZ\}$ around the Y -axis |
| γ | The angle of $\{F-X_F Y_F Z_F\}$ relative to $\{D-X_D Y_D Z_D\}$ around the X_D axis |

could walk independently. In the stance phase, the control software switched to position control to guide the limb to move (Bernhardt et al., 2005). Ju et al. developed a hybrid position/force controller for the rehabilitation robot combined with fuzzy logic to track the desired force along the preset motion direction (Ju et al., 2005). Valera et al. developed a hybrid control scheme based on the position/force information, which makes it possible to perform different lower limb rehabilitation exercises (Valera et al., 2017). However, due to the position/force dynamic relationship being adjusted to increase robot compliance in impedance control, it increases the difficulty of guaranteeing the trajectory tracking effect of the robot in lower limb rehabilitation training (Lv et al., 2017). The common position/force hybrid control strategy allows patients to bear a certain amount of resistance close to the preset trajectory, which limits the active participation of patients (Rivas-Blanco et al., 2013).

Aiming at the shortcomings of most existing control strategies for lower limb rehabilitation robots that are difficult to guarantee trajectory tracking effect and active participation of the patient, a force/position-based velocity control (FPVC) strategy is proposed for the hybrid end-effector lower limb rehabilitation robot (HE-LRR) in this paper. On one hand, HE-LRR has the advantages of a large workspace and strong bearing capacity and is also suitable for experimental verification on subjects with different body dimensions. On the other hand, HE-LRR can guide the lower limbs to perform three-dimensional spatial movements, achieving various typical lower limb rehabilitation exercises such as MOTomed therapy and continuous passive motion (CPM) therapy. Experimental studies have been conducted to verify the rationality of the FPVC strategy under MOTomed and CPM modes. This paper is organized as follows. In the Materials and Methods section, the configuration of HE-LRR is introduced and the

FPVC strategy design is proposed. Then the experimental platform is described. In the Results section, the validation experiments are conducted, including trajectory measurement experiments, force and velocity measurement experiments, and active participation experiments. In the Conclusions and Discussion section, the summary and prospect of the FPVC strategy are presented.

2 Materials and methods

2.1 Configuration of HE-LRR

HE-LRR consists of a base frame, connecting rods, linear actuators, robot joints, and pedal units, as shown in Figure 1A. The pedal unit is the end effector of HE-LRR, consisting of a foot pedal, a force sensor, connecting plates, and a pedal shaft, as shown in Figure 1B.

Figure 1C shows the robot configuration diagram. The origin of the fixed coordinate system $\{O-XYZ\}$ lies at the intersection of the two rotational auxiliary axes of the universal joint. The X -axis coincides with one axis of the universal joint and along the OA_2 direction. The Y -axis coincides with another axis of the universal joint and along the OA_1 direction. The direction of the Z -axis is determined by the right-hand screw rule. Moving coordinate system $\{B-X_B Y_B Z_B\}$ has its origin at the OD rod, X_B axis along the BB_2 direction, and Y_B axis along the BB_1 direction. The moving coordinate system $\{D-X_D Y_D Z_D\}$ is established with the X_D axis along the axis of the revolute joint D and the Z_D axis along the OD direction. Point F represents the midpoint of the robot end effectors (pedal units). The X_F axis of the moving coordinate system $\{F-X_F Y_F Z_F\}$ is parallel to the X_D direction, and the Z_F axis is along the DF direction.

2.2 Inverse Jacobian analysis

In this subsection, the parameter symbols and descriptions of the robot configuration are shown in Table 1. According to the geometric relationships in Figure 1C, the coordinates of point F can be expressed as follows:

$$\begin{cases} F_x = l_2 \sin \beta \cos(\alpha + \gamma) + l_1 \cos \alpha \sin \beta \\ F_y = -l_2 \sin(\alpha + \gamma) - l_1 \sin \alpha \\ F_z = l_2 \cos \beta \cos(\alpha + \gamma) + l_1 \cos \alpha \cos \beta \end{cases} \quad (1)$$

According to Eq. 1, the rotation angles α , β and γ can be expressed as:

$$\begin{cases} \alpha = -\arccos\left(\frac{l_1^2 + F_x^2 + F_y^2 + F_z^2 - l_2^2}{2l_1\sqrt{F_x^2 + F_y^2 + F_z^2}}\right) - \arctan\left(\frac{F_y}{F_z} \cos \beta\right) \\ \beta = \arctan\left(\frac{F_x}{F_z}\right) \\ \gamma = \arccos\frac{F_x^2 + F_y^2 + F_z^2 - l_2^2 - l_1^2}{2l_1 l_2} \end{cases} \quad (2)$$

Taking the derivative of time on both sides of Eq. 2, the mapping relationship between the angular velocities and the velocity components of the robot end effector can be expressed in the following matrix form:

$$\begin{bmatrix} \dot{\alpha} \\ \dot{\beta} \\ \dot{\gamma} \end{bmatrix} = J_1 \begin{bmatrix} \dot{F}_x \\ \dot{F}_y \\ \dot{F}_z \end{bmatrix} = \begin{bmatrix} \frac{\partial \alpha}{\partial F_x} & \frac{\partial \alpha}{\partial F_y} & \frac{\partial \alpha}{\partial F_z} \\ \frac{\partial \beta}{\partial F_x} & \frac{\partial \beta}{\partial F_y} & \frac{\partial \beta}{\partial F_z} \\ \frac{\partial \gamma}{\partial F_x} & \frac{\partial \gamma}{\partial F_y} & \frac{\partial \gamma}{\partial F_z} \end{bmatrix} \begin{bmatrix} \dot{F}_x \\ \dot{F}_y \\ \dot{F}_z \end{bmatrix} \quad (3)$$

where J_1 is the velocity Jacobian matrix between the angular velocities and velocity components of the robot end effector.

Establish the following closed-loop vector equation in the fixed coordinate system $\{O-XYZ\}$

$$l_{OB} + {}^O_B R n_i = m_i + A_i B_i \quad (i = 1, 2) \quad (4)$$

where ${}^O_B R$ is the rotation matrix from $\{B-X_B Y_B Z_B\}$ to $\{O-XYZ\}$, n_i is the position vector of B_i in the coordinate system $\{B-X_B Y_B Z_B\}$, m_i is the position vector of A_i in the coordinate system $\{O-XYZ\}$, l_{OB} and $A_i B_i$ are the vectors of OB and $A_i B_i$ in the fixed coordinate system.

Substituting mechanical parameters into Eq. 4 and simplifying to get expressions of the linear actuator lengths l_{01} and l_{02}

$$\begin{cases} l_{01} = \sqrt{a_1^2 + b_1^2 + l_{OB}^2 - 1a_1 b_1 \cos \alpha + 2l_{OB} a_1 \sin \alpha} \\ l_{02} = \sqrt{a_2^2 + b_2^2 + l_{OB}^2 - 1a_2 b_2 \cos \beta + 2l_{OB} a_2 \sin \beta} \end{cases} \quad (5)$$

According to the Cosine Theorem, we can get Eq. 6

$$\cos \angle C_2 D C_3 = \frac{b_3^2 + m_2^2 + m_1^2 + a_3^2 - l_{03}^2}{2\sqrt{b_3^2 + m_2^2} \sqrt{m_1^2 + a_3^2}} \quad (6)$$

γ angle can be solved as Eq. 7

$$\gamma = \pi - \arccos \frac{b_3^2 + m_2^2 + a_3^2 + m_1^2 - l_{03}^2}{2\sqrt{b_3^2 + m_2^2} \sqrt{a_3^2 + m_1^2}} \quad (7)$$

Hence, the linear actuator length l_{03} can be expressed as

$$l_{03} = \sqrt{a_3^2 + b_3^2 + m_1^2 + m_2^2 + 2\sqrt{m_1^2 + a_3^2} \sqrt{m_2^2 + b_3^2} \cos \left(\gamma + \arctan \frac{b_3}{m_2} + \arctan \frac{a_3}{m_1} \right)} \quad (8)$$

The relationship between linear actuator velocities and angular velocities can be obtained by taking the derivative of time on both sides of Eqs 5, 8:

$$\begin{cases} \dot{l}_{01} = \frac{a_1 l_{OB} \cos \alpha + a_1 b_1 \sin \alpha}{l_{01}} \dot{\alpha} \\ \dot{l}_{02} = \frac{a_2 l_{OB} \sin \alpha \sin \beta}{l_{02}} \dot{\alpha} \\ + \frac{a_2 b_2 \sin \beta - a_2 l_{OB} \cos \alpha \cos \beta}{l_{02}} \dot{\beta} \\ \dot{l}_{03} = \frac{\sin \left(\gamma + \arctan \frac{b_3}{m_2} + \arctan \frac{a_3}{m_1} \right) \sqrt{a_3^2 + m_1^2} \sqrt{b_3^2 + m_2^2}}{l_{03}} \dot{\gamma} \end{cases} \quad (9)$$

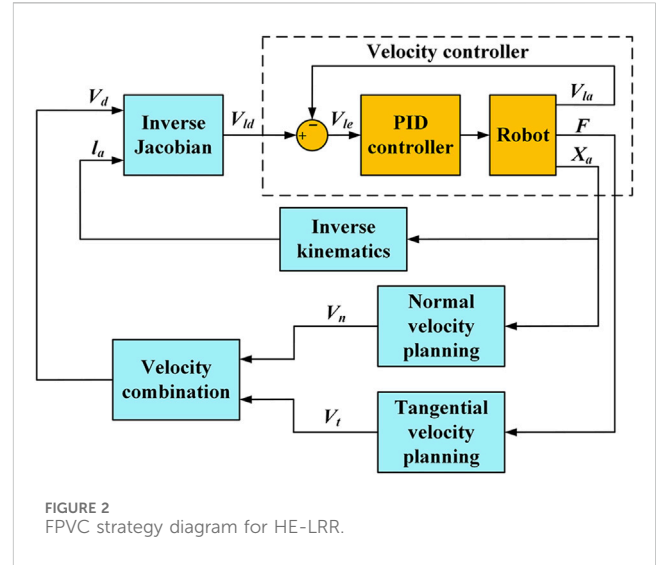


FIGURE 2 FPVC strategy diagram for HE-LRR.

J_2 is used to represent the Jacobian matrix between the linear actuator velocities and angular velocities. Eq. 9 can be written in the following matrix form:

$$\begin{bmatrix} \dot{l}_{01} \\ \dot{l}_{02} \\ \dot{l}_{03} \end{bmatrix} = J_2 \begin{bmatrix} \dot{\alpha} \\ \dot{\beta} \\ \dot{\gamma} \end{bmatrix} = \begin{bmatrix} J_{11} & 0 & 0 \\ J_{21} & J_{22} & 0 \\ 0 & 0 & J_{33} \end{bmatrix} \begin{bmatrix} \dot{\alpha} \\ \dot{\beta} \\ \dot{\gamma} \end{bmatrix} \quad (10)$$

where

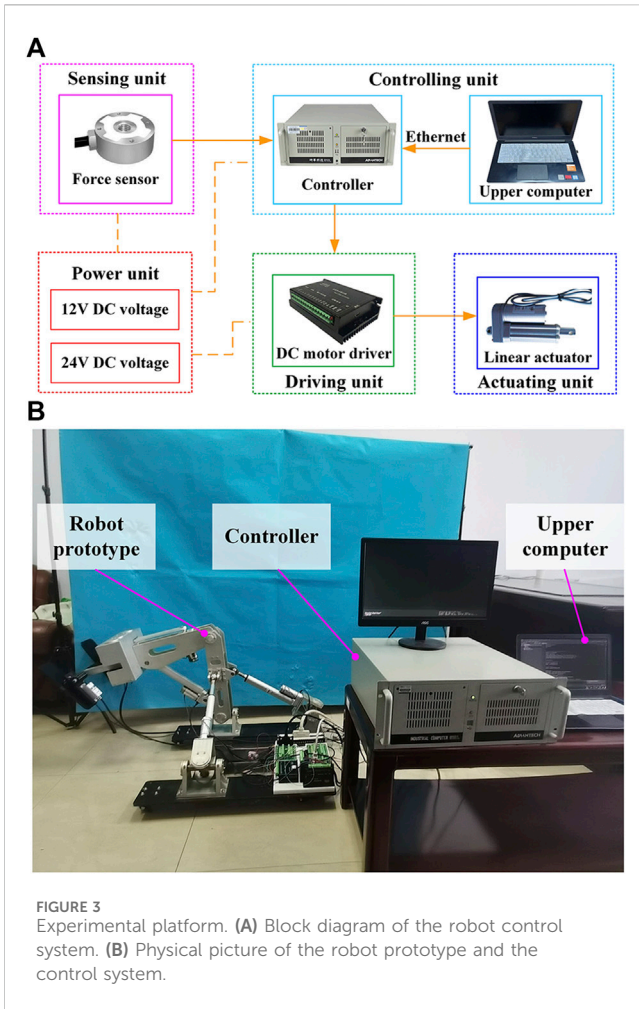
$$\begin{cases} J_{11} = \frac{a_1 l_{OB} \cos \alpha + a_1 b_1 \sin \alpha}{l_{01}} \\ J_{21} = \frac{a_2 l_{OB} \sin \alpha \sin \beta}{l_{02}} \\ J_{22} = \frac{a_2 b_2 \sin \beta - a_2 l_{OB} \cos \alpha \cos \beta}{l_{02}} \\ J_{33} = \frac{\sin \left(\gamma + \arctan \frac{b_3}{m_2} + \arctan \frac{a_3}{m_1} \right) \sqrt{a_3^2 + m_1^2} \sqrt{b_3^2 + m_2^2}}{l_{03}} \end{cases}$$

The inverse Jacobian matrix J_i can be used to represent the mapping relationship between the linear actuator velocities and the velocity components of the robot end effector. Combined with Eqs 3, 10, we can obtain Eq. 11:

$$\begin{bmatrix} \dot{l}_{01} \\ \dot{l}_{02} \\ \dot{l}_{03} \end{bmatrix} = J_i \begin{bmatrix} \dot{F}_x \\ \dot{F}_y \\ \dot{F}_z \end{bmatrix}, J_i = J_1 J_2 \quad (11)$$

2.3 FPVC strategy design

Figure 2 shows the FPVC strategy diagram for HE-LRR. The end effector's actual three-dimensional position coordinate information X_a is used to plan the normal velocity (NV) V_n of HE-LRR, and man-machine contact force (MCF) F is used to plan the tangential velocity (TV) V_t of HE-LRR. The NV and TV are combined as the



end effector's desired velocity V_d . The actual position of each linear actuator l_a is calculated by inverse kinematics. Combined with the desired velocity V_d and the actual linear actuator position l_a , the desired velocity of each linear actuator V_{ld} is calculated by inverse Jacobian and is sent to the velocity controller of the FPVC strategy. The calculation process of inverse kinematics is shown in the literature (Wang et al., 2022). NV planning and TV planning are introduced in this subsection in detail.

HE-LRR assists the patient's lower limbs in performing rehabilitation exercises under the constraint trajectory through end traction, so it is essential that the end effector can move along the reference trajectory in space. When the end effector deviates from the reference trajectory, the desired NV is planned to reduce the deviation. P_1 is the actual end point of the end effector of HE-LRR, and P_2 is the closest point on the reference trajectory to point P_1 . The desired NV direction is along the direction of P_1P_2 and points towards P_2 .

The end effector's desired NV can be calculated by Eq. 12:

$$V_n = k_n d \tag{12}$$

where k_n is the NV coefficient, and d is the shortest distance from point P_1 to the reference trajectory.

The mapping function between TV and MCF is planned as a piecewise function, including the initial segment sub-function, linear segment sub-function and parabolic segment sub-function. When MCF is less than the initial threshold F_b , it is considered that MCF

is caused by random factors such as mechanical jitter, and cannot represent the patient's active intention, and the desired TV is equal to zero. When the MCF exceeds the initial threshold F_i and falls below the linear threshold F_b , it is considered that MCF can reflect the patient's movement intention. The mapping function is planned as a linear correlation between the desired TV and MCF. When MCF exceeds the linear threshold F_b , the slope of the mapping function needs to decrease based on safety consideration, and the mapping relationship between TV and MCF is planned as a parabolic sub-function.

According to the above parameters and settings, the initial segment sub-function is:

$$V_t = 0 (F \leq F_i) \tag{13}$$

The linear segment sub-function is:

$$V_t = k_l F - k_l F_i (F_i < F \leq F_b) \tag{14}$$

where k_l represents the linear segment slope.

The linear threshold F_l can be expressed as follows:

$$F_l = \frac{V_{lm} + k_l F_i}{k_l} \tag{15}$$

where V_{lm} represents the maximum linear velocity.

The parabolic equation whose focus is on the F -axis is chosen for the planning of the third segment sub-function. The parabolic sub-function can be written as:

$$V_t = \sqrt{2p(F - q)} \tag{16}$$

where q is the F -axis translation distance, and p represents the distance from the focus to the directrix of the parabola.

To meet the piecewise function's continuity requirement, the point (F_b, V_{lm}) is the intersection point of the linear segment and the parabolic segment, thus:

$$V_{lm} = \sqrt{2p(F_b - q)} \tag{17}$$

The parabolic slope at the point (F_b, V_{lm}) is set to half the linear slope, thus:

$$\frac{k_l}{2} = \frac{p}{\sqrt{2p(F_b - q)}} \tag{18}$$

Combined with Eqs 15–18, the parabolic segment sub-function can be expressed as:

$$V_t = \sqrt{k_l V_{lm} (F - F_i)} (F > F_b) \tag{19}$$

Combined with Eqs 13, 14, 19, the piecewise function can be expressed as:

$$V_t = \begin{cases} 0 & F \leq F_i \\ k_l F - k_l F_i & F_i < F \leq \frac{V_{lm} + k_l F_i}{k_l} \\ \sqrt{k_l V_{lm} (F - F_i)} & F > \frac{V_{lm} + k_l F_i}{k_l} \end{cases} \tag{20}$$

It can be seen from Eq. 20 that the mapping function between TV and MCF can be determined by three parameters, including the initial threshold F_b , the linear segment slope k_l , and the maximum linear velocity V_{lm} .

TABLE 2 Basic information on healthy subjects.

| Number | Height (mm) | Weight (kg) | Thigh length (mm) | Calf length (mm) |
|--------|-------------|-------------|-------------------|------------------|
| 1 | 1720 | 75 | 430 | 400 |
| 2 | 1670 | 78 | 405 | 385 |
| 3 | 1690 | 72 | 415 | 400 |

2.4 Experimental platform

Figure 3A illustrates the block diagram of the lower limb rehabilitation robot's control system, which includes the controlling, sensing, driving, actuating, and power units. A personal computer (Advantech, IPC610, CN) serves as the controller. In addition to receiving commands from the upper computer (Dell, Vostro 5370, USA), the IPC can also receive signals from force sensors (HUILIZHI, LZ-SWF40, 0–300 N, $\pm 0.3\%$ F.S., CN) and encoders. The motor drivers (Magicon Intelligent, MC-FBLD-6600, 9–36 V, 12 A, CN) receive commands from the controller to accomplish the telescopic movement of the linear actuators (YCMC, LEC606, 210 mm, 0–450 N, CN). An incremental encoder records the DC motor's actual position as it moves to facilitate the linear actuator's velocity closed-loop control. The angle sensors, encoders, and motor drivers are powered by the power unit that supplies 12 V or 24 V DC voltage.

As shown in Figure 3B, the prototype of HE-LRR has been manufactured, and the control system has been built. The robot's base frame is equipped with casters with brakes to facilitate robot movement and improve stability. Rehabilitation training is performed with the patient's feet on the pedal units. According to the procedure (CRRC-IEC-RF-SC-005-01) approved by the China Rehabilitation Research Center, three healthy subjects were recruited to participate in the experiments. Basic information about the subjects is presented in Table 2. During the experiments, none of the subjects reported discomfort.

3 Results

To validate the feasibility of the FPVC strategy, trajectory measurement experiments, force and velocity measurement experiments, and active participation experiments are carried out in this section.

3.1 Trajectory measurement experiments

The active training based on the FPVC strategy is carried out under the constraint trajectory, which makes it possible for patients to obtain a large range of joint activities. The trajectory measurement experiments of HE-LRR are carried out under MOTomed mode (Figure 4A) and CPM mode (Figure 4B). The constraint trajectories for the above two modes are a circular trajectory and a linear trajectory, respectively. The subject's feet are connected with the end effector through Velcro tapes. During the experiment, the actual positions of the linear actuators are

recorded, and the actual end position of HE-LRR can be calculated through the forward kinematics of the robot. Each group of experiments was conducted for 10 min. In subsections 3.1 and 3.2, 10 s of data were displayed to more clearly represent the results.

The trajectory measurement experimental results of HE-LRR in MOTomed mode are shown in Figure 5. The reference trajectory parameters are set as shown in Figure 5A: the center coordinates $(x_0, y_0, z_0) = (0, -670, 470)$, the radius is 100.00 mm. When the initial position is outside the circular trajectory, the initial point is set to $(x_0, y_0, z_0) = (0, -670, 620)$. When the initial position is inside the circular trajectory, the initial point is set to $(x_0, y_0, z_0) = (0, -670, 520)$. It can be seen that during the experiment, the end position of the robot quickly approaches the reference trajectory first, and then the approaching velocity slows down. Finally, the end effector's actual trajectory has a good coincidence degree with the reference trajectory. The minimum distance between the end effector's actual position and the reference trajectory is defined as the actual position error of the robot. Figure 5B shows the robot's actual position errors under MOTomed mode. The position errors of the robot are different due to the difference in the starting point. The initial position errors of experimental Group A and Group B are 50 mm and -50 mm, respectively. The positive error value indicates that the initial point is outside the circular trajectory, and the negative value indicates that the initial point is inside the circular trajectory. At about 2.91 s, the position error of experimental Group A decreases to 5.00 mm. At about 1.70 s, the position error of experimental Group B becomes -5.00 mm. After about 4 s, the end error of the robot decreases to a small range, which suggests that the trajectory tracking effect of the end effector shows good accuracy and stability under different initial position errors.

The trajectory measurement experimental results of HE-LRR in CPM mode are shown in Figure 6. The reference trajectory parameters are set as shown in Figure 6A: the linear trajectory passes through $(x_0, y_0, z_0) = (0, -810, 290)$, and the inclination angle is 10° . When the starting point is above the linear trajectory, the initial point is set as $(x_0, y_0, z_0) = (0, -725, 400)$. When the starting point is below the linear trajectory, the initial point is set as $(x_0, y_0, z_0) = (0, -720, 215)$. It can be seen that the end position of the robot approaches the reference trajectory quickly initially. After the switch from forward motion to backward motion, the end position of the robot still gets close to the reference trajectory. Finally, the actual trajectory has a good coincidence with the reference trajectory. According to Figure 6B, when the starting point is above the linear trajectory, the initial position error is -93.57 mm, and after 2.35 s, the position error becomes -9.36 mm (approximately 10% of the initial position error), and the final position error is in a small range. When the starting point is below the linear trajectory, the initial position error is 89.48 mm. After 2.31 s, the position error

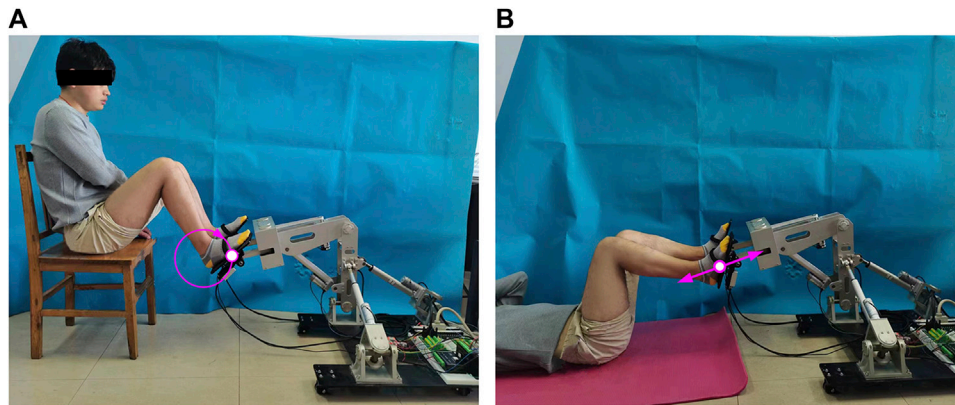


FIGURE 4 Field diagram of trajectory measurement experiments of HE-LRR. (A) MOTomed mode. (B) CPM mode.

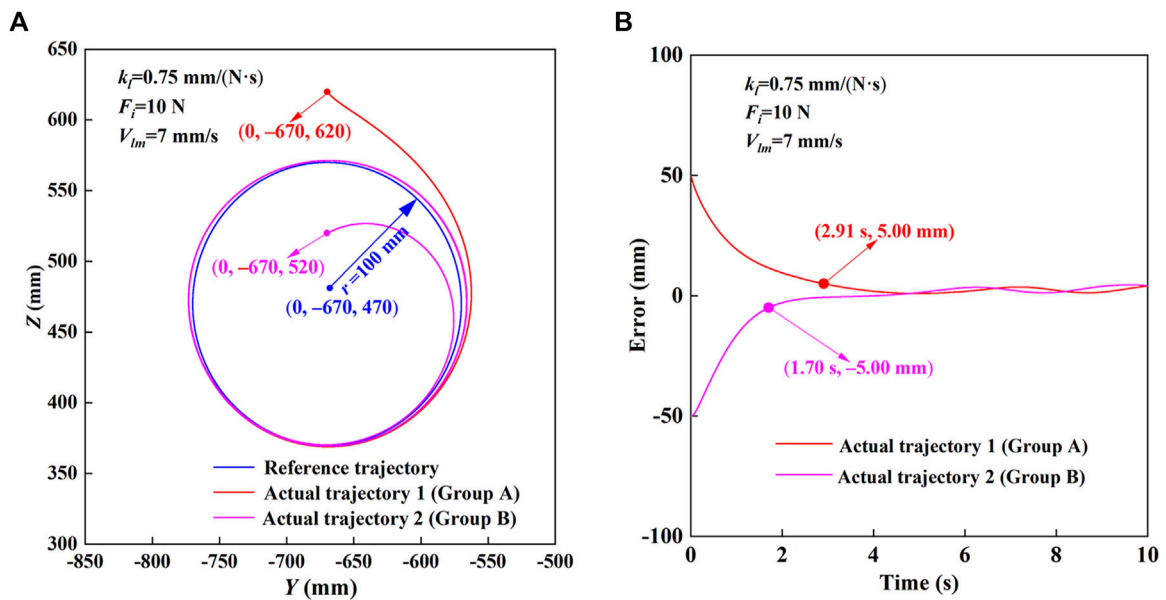


FIGURE 5 Trajectory measurement experimental results of HE-LRR in MOTomed mode. (A) Comparison of the reference trajectory and actual trajectory. (B) Actual position errors.

decreases to 8.95 mm (approximately 10% of the initial position error), and the final position error is in a small range. In conclusion, the robot based on the FPVC strategy can realize the rehabilitation training of the predetermined trajectory with good accuracy and stability under the MOTomed and CPM modes.

3.2 Force and velocity measurement experiments

In active training, the robot system recognizes the motion intention of the patient by detecting the force applied at the end effector, and assists the lower limb in realizing the rehabilitation training through the

actuating unit. The parameter settings of the circular trajectory and the linear trajectory are consistent with those in Section 5.1. The control strategy parameters are set as follows: the initial threshold $F_t = 10$ N, the maximum linear velocity $V_{lm} = 7$ mm/s, and the linear segment slope $k_t = 0.75$ mm/(N·s). Based on the forward kinematics of the robot, the end effector's actual position can be calculated from the actual positions of linear actuators. After the differential calculation, the end effector's actual velocity can be obtained.

Figure 7 shows the experimental results of the force and velocity of the robot in MOTomed mode. In MOTomed mode, clockwise and counterclockwise motions are studied, respectively. In the clockwise motion (Figure 7A), when the MCF value is positive, the desired velocity is also non-negative and the fluctuation trend of

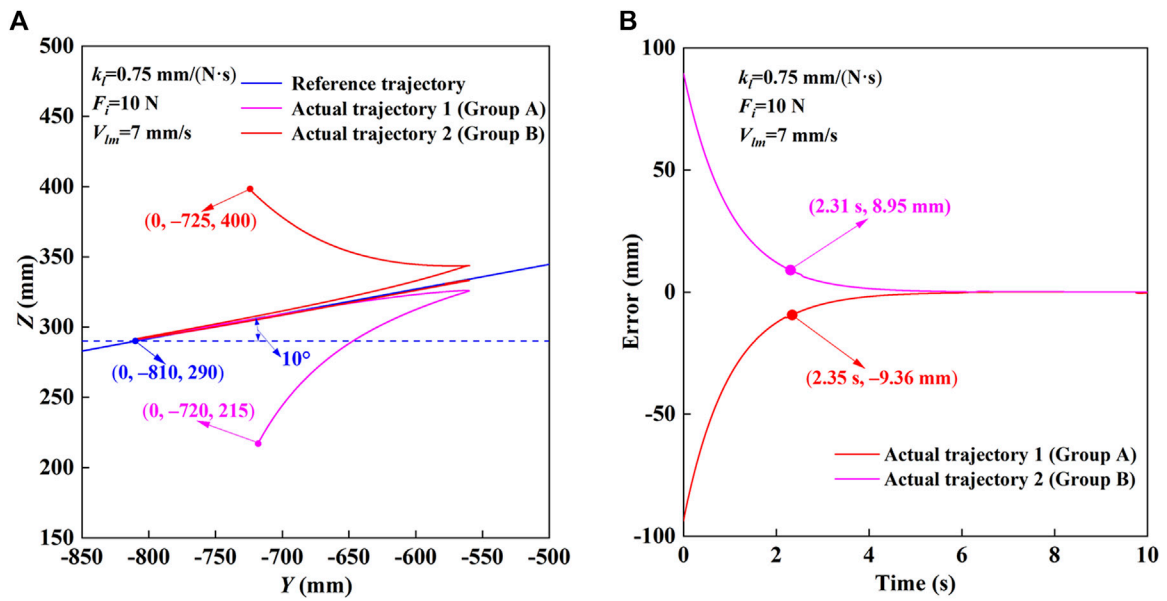


FIGURE 6 Trajectory measurement experimental results of HE-LRR in CPM mode. (A) Comparison of the reference trajectory and actual trajectory. (B) Actual position errors.

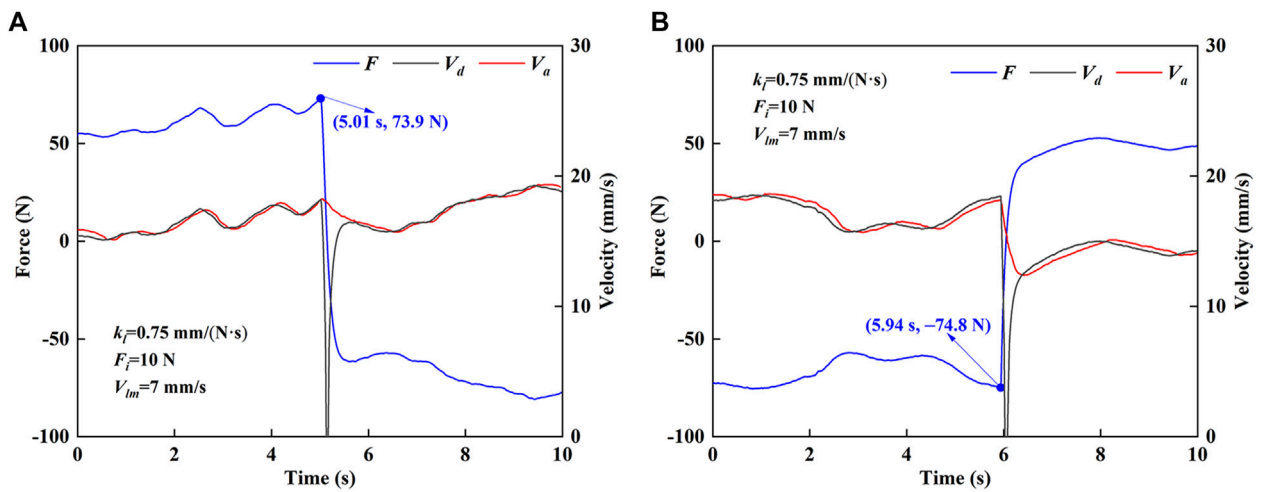


FIGURE 7 Force and velocity results of HE-LRR in MOTomed mode. (A) Clockwise motion. (B) Counterclockwise motion.

the desired velocity is consistent with MCF. When the MCF value is negative, the desired velocity is non-negative and the fluctuation trend of the desired velocity is opposite to that of MCF. After 5.01 s, the MCF rapidly changes from compression force (73.9 N) to tension force. At this time, the desired velocity rapidly decreases to 0 mm/s and then rapidly increases. In the counterclockwise motion (Figure 7B), when the MCF value is negative, the desired velocity is non-negative and the fluctuation trend of the desired velocity is opposite to that of the MCF. When the MCF value is positive, the desired velocity is non-negative and the desired velocity

and MCF have the same fluctuation trend. From 5.94 s, the MCF quickly changes from tension force (-74.8 N) to compression force, and the desired velocity shows a changing law of rapid decrease and rapid increase. When the desired velocity change rate is low, the end effector's actual velocity can better follow the desired velocity. When the desired velocity curve has a significant mutation, the changing trend of the actual velocity is quite different and the velocity change is relatively slow. Since it is expected to avoid the velocity mutation during the rehabilitation training, it is beneficial that the actual velocity of the robot can keep relatively stable.

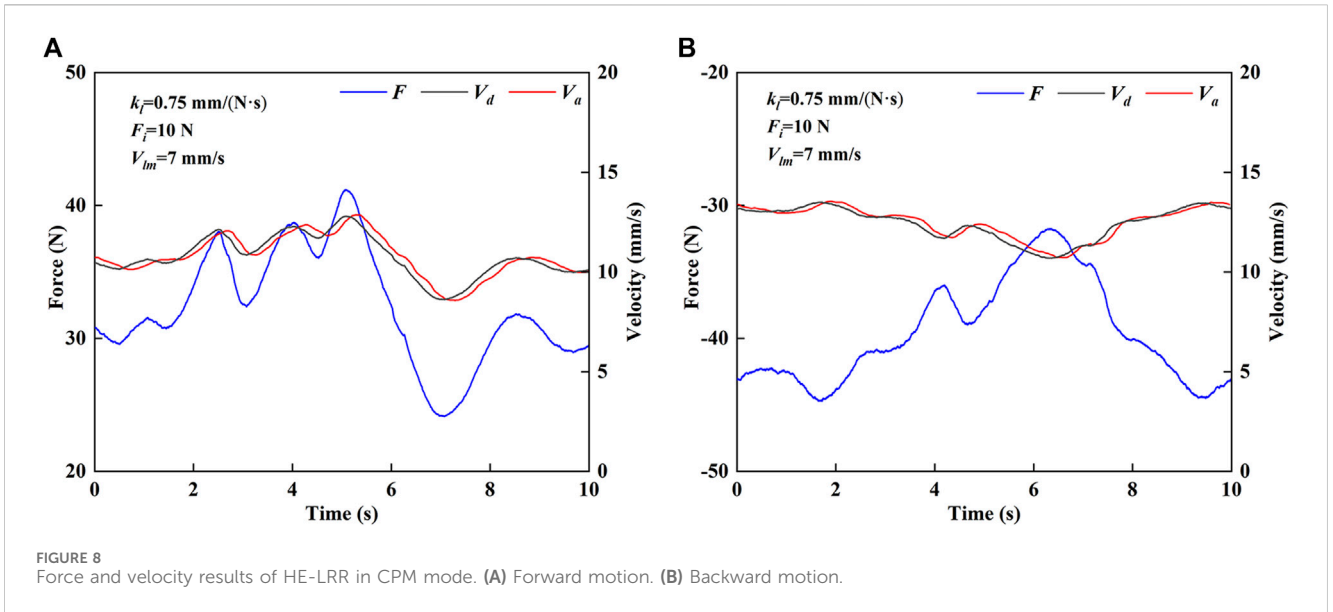


FIGURE 8 Force and velocity results of HE-LRR in CPM mode. (A) Forward motion. (B) Backward motion.

Figure 8 shows the experimental results of the force and velocity of the robot in CPM mode. In CPM mode, it is divided into forward motion and backward motion for research. As shown in Figure 8A, in the forward motion, the value of MCF is positive, and the desired velocity is non-negative. The desired velocity and the MCF show similar fluctuation trends. As shown in Figure 8B, in the backward motion, the MCF value is negative, and the desired velocity is non-negative. The desired velocity and the MCF show opposite fluctuation trends. It can be seen that the end effector's actual velocity has good following ability to the desired velocity in both forward and backward motions, which indicates that the robot motion is very sensitive to the change of the MCF, and can adapt to the active movement intention of the subject.

3.3 Active participation experiments

In order to study the FPVC strategy parameters' effects on the active participation of subjects, this section conducts experimental research on active participation. We recruited three healthy subjects to participate in the MOTomed and CPM modes. All subjects agreed to include personal data in the study before the experiments. Each subject participated in 30 active training tasks under different control strategy parameters.

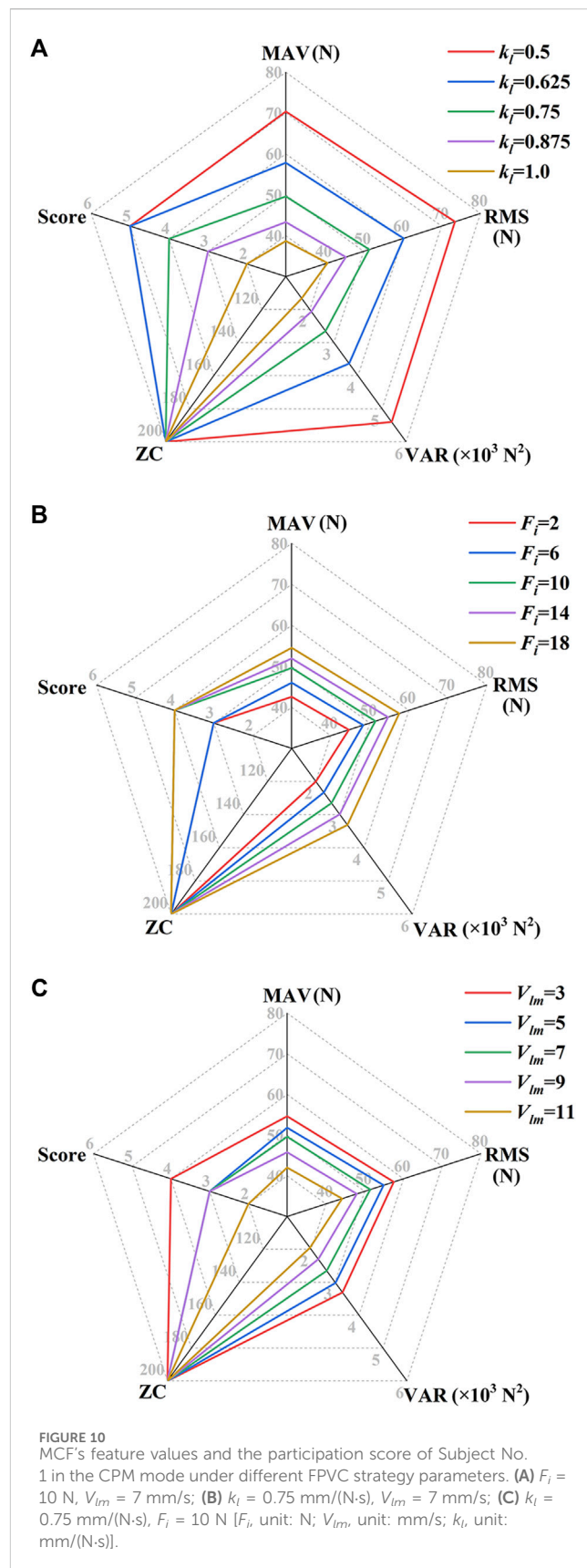
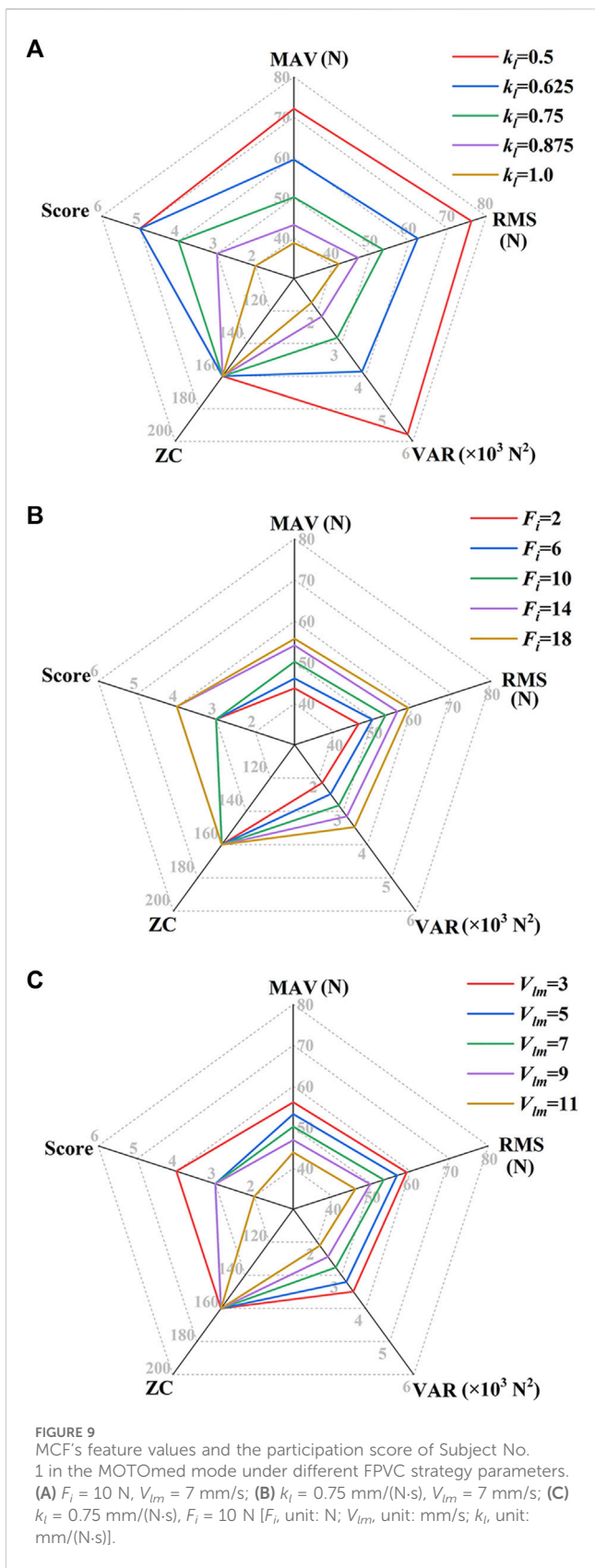
During active participation experiments, subjects were required to complete a certain number of tasks in 10 minutes. For the MOTomed mode, eight cycles of training needed to be completed per minute; For the CPM mode, it was required to complete ten cycles of training per minute, and each subject could have a rest and physical recovery after completing each task. After completing the training task, the subject was asked to take a questionnaire on the subjective feeling and the participation score. When the subject's subjective feeling was boredom, relaxation, excitement, stress, or frustration, the corresponding participation score was 1, 2, 3, 4, or 5, respectively.

During the experiment, the MCF signal collected by the force sensor was filtered by the Kalman filter, and the objective feature values of root mean square (RMS), mean absolute value (MAV), variance (VAR), and zero crossing (ZC) were extracted from the processed MCF signal. RMS and MAV are statistics which can reflect the MCF signal's effective value and average strength. VAR can provide information regarding the signal's power. ZC represents the number of times the signal crosses the zero line, reflecting the number of times the MCF signal switches between tension force and compression force and can be used to calculate the number of training cycles. The additional threshold judgment is introduced to reduce the impact of signal noise on the ZC. The feature values can be calculated according to Eq. 21:

$$\left\{ \begin{array}{l}
 \text{MAV} = \frac{1}{N} \sum_{i=1}^N |x_i| \\
 \text{RMS} = \sqrt{\frac{\sum_{i=1}^N x_i^2}{N}} \\
 \text{VAR} = \frac{1}{N-1} \sum_{i=1}^N x_i^2 \\
 \text{ZC} = \sum_{i=1}^{N-1} f(i) \\
 f(i) = \begin{cases} 1 & x_i x_{i+1} < 0, \text{ and } |x_i - x_{i+1}| > \text{threshold} \\ 0 & \text{otherwise} \end{cases}
 \end{array} \right. \quad (21)$$

where x_i represents the i th value of the MCF signal, and N represents the number of the data values.

Figure 9 shows the MCF's feature values and the participation score of Subject No. 1 in the MOTomed mode under different FPVC strategy parameters. When F_i and V_{lm} are constant: $F_i = 10 \text{ N}$ and $V_{lm} = 7 \text{ mm/s}$ (Figure 9A), ZC values are 160, indicating that the subject has completed 80 cycles of MOTomed training. MAV, RMS and VAR increase with the



decrease of k_l ; When $k_l = 0.5$ mm/(N·s), MAV, RMS and VAR achieve maximum values, and the participation score is 5, indicating that the subjective feeling is frustration. When k_l

and V_{lm} are constant: $k_l = 0.75$ mm/(N·s) and $V_{lm} = 7$ mm/s (Figure 9B), MAV, RMS, VAR increase with the increase of F_i , and ZC value remains unchanged. When $F_i = 18$ N, the objective

TABLE 3 PSO-BP algorithm parameter setting.

| Parameter | Parameter value |
|------------------------------------------|--------------------|
| Training number | 1000 |
| Learning rate | 0.01 |
| Minimum error | 1×10^{-5} |
| Momentum factor | 0.01 |
| Minimum gradient | 1×10^{-6} |
| Swarm size | 30 |
| Space dimension | 82 |
| Maximal number of iterations | 100 |
| Inertia weight | 0.9 |
| Acceleration coefficients (c_1, c_2) | (2, 2) |

indicators achieve the maximum values, and the participation score is 4. When k_l and F_i are constant: $k_l = 0.75 \text{ mm}/(\text{N}\cdot\text{s})$ and $F_i = 10 \text{ N}$ (Figure 9C), MAV, RMS and VAR increase with the decrease of V_{lm} . When $V_{lm} = 3 \text{ m/s}$, MAV, RMS and VAR achieve maximum values, and the participation score is 4. When $V_{lm} = 11 \text{ m/s}$, MAV, RMS and VAR achieve minimum values, and the participation score is 2.

Figure 10 shows the MCF's feature values and the participation score of Subject No. 1 in the CPM mode under different FPVC strategy parameters. When F_i and V_{lm} are fixed: $F_i = 10 \text{ N}$ and $V_{lm} = 7 \text{ mm/s}$ (Figure 10A), the ZC value is 200, indicating that the subject has completed 100 cycles of CPM training. MAV, RMS and VAR have similar change laws as in the MOTomed mode. When k_l and V_{lm} are constant: $k_l = 0.75 \text{ mm}/(\text{N}\cdot\text{s})$ and $V_{lm} = 7 \text{ mm/s}$ (Figure 10B), the ZC value is 200. When $F_i = 18 \text{ N}$, MAV, RMS and VAR achieve maximum values, and the participation score is 4. When k_l and F_i are constant: $k_l = 0.75 \text{ mm}/(\text{N}\cdot\text{s})$ and $F_i = 10 \text{ N}$ (Figure 10C), the ZC value is also 200. When $V_{lm} = 3 \text{ mm/s}$, the objective indicators achieve maximum values, and the participation score is 4.

Based on the above experimental results, the mapping relationship between the objective indicators (the feature values of the MCF signal) and the subjective indicators (participation scores given by the subjects) was studied to realize the prediction from the objective indicators to the subjective indicators. The particle swarm optimization-backpropagation (PSO-BP) algorithm was selected for the regression prediction of active participation. The algorithm parameter setting is shown in Table 3. Three subjects participated in the active training of the MOTomed and CPM modes under different control strategy parameters. The feature values of MCF were taken as the training set's input parameters X_s , and the questionnaire scores of subjects for different training tasks were taken as the output parameters Y_s of the training set.

Each subject participated in 10 groups of training under different control strategy parameters. After the experiments, they took the questionnaire survey. The feature values of MCF were taken as input parameters X_t of the testing set, and the active participation scores of the questionnaire were taken as the actual output parameters Y_t of the testing set. Using the trained prediction

model of active participation, the predicted values Y_p were predicted from the input parameters X_t . The comparison between the actual value and the predicted value of the testing sets for different subjects is shown in Figure 11.

The participation score of the subject in the testing set is an integer score of "1, 2, 3, 4, 5". Because the subjects have different evaluation criteria for participation, the dynamic trends of training data are also different. The experimental results show that the active participation scores predicted by the PSO-BO algorithm are close to the actual values. If the absolute error value between the actual value and the predicted value is less than 0.25, it is regarded as accurate; Otherwise, it is regarded as inaccurate. Then the prediction accuracy rate for Subject No. 1 is 60% (Figure 11A), that for Subject No. 2 is 80% (Figure 11B), and that for Subject No. 3 is 70% (Figure 11C). If the absolute error value between the actual value and the predicted value is less than 0.5, it is regarded as accurate; Otherwise, it is regarded as inaccurate. Then the prediction accuracy for three subjects can reach 100%. The above results show that subjects' active participation in training tasks can be predicted from the MCF's feature values, and the prediction accuracy can meet the prediction requirements from objective feature values to subjective indicators.

4 Conclusion and discussion

In this paper, a force/position-based velocity control strategy was proposed for HE-LRR to meet the demands of trajectory tracking effect and active participation of lower limb rehabilitation robots. The end effector's velocity planning was introduced in detail. Experimental studies were carried out on the control strategy with the following conclusions:

- (1) The trajectory measurement experiments of HE-LRR were carried out under two training modes. The results showed that the end effector could approach the reference trajectory in a short time when the starting points of the end effector were different (inside the circular trajectory, outside the circular trajectory, above the linear trajectory, below the linear trajectory), which proved that the FPVC strategy is beneficial for subjects to achieve active rehabilitation training under accurate trajectories.
- (2) The force and velocity measurement experiments of HE-LRR were carried out in two training modes. The results showed that the actual velocity of the end effector possessed good following performance compared with the desired velocity, which reflected that the robot could adapt to the changes of MCF, and proved the rationality of velocity planning in the FPVC strategy.
- (3) Active participation experiments were conducted under different control strategy parameters, and the prediction of the active participation was performed using the PSO-BP algorithm. The results showed that the active participation of subjects could be adjusted by the control strategy parameters, and the active participation score could be predicted accurately from the MCF's feature values.

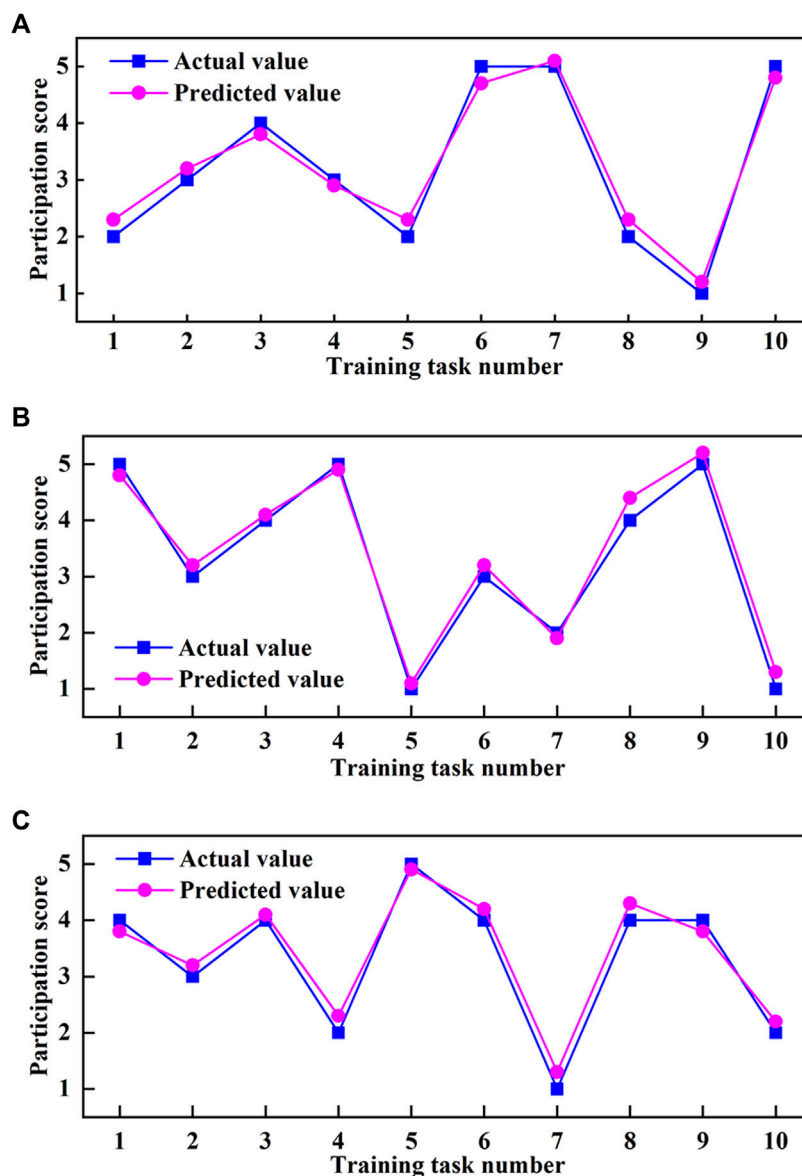


FIGURE 11 Comparison between the actual value and the predicted value of active participation score. (A) Subject No. 1. (B) Subject No. 2. (C) Subject No. 3.

Although the rationality and feasibility of the FPVC strategy have been experimentally verified on the HE-LRR system, there are still some things that could be improved in the research work. For example, the FPVC strategy was mainly validated on the end-effector lower limb rehabilitation robot under MOTomed and CPM modes, which are training modes in the sagittal plane, and the experimental validation of the FPVC strategy was conducted by recruiting a series of healthy subjects. Our future research work will mainly focus on carrying out three-dimensional spatial trajectory verification and on the exoskeleton-type lower limb rehabilitation robot to improve the robot's functionality and practicality, and conducting clinical experiments to study patients' experience and active participation under the FPVC strategy.

Data availability statement

The raw data supporting the conclusion of this article will be made available by the authors, without undue reservation.

Ethics statement

The studies involving humans were approved by the China Rehabilitation Research Center. The studies were conducted in accordance with the local legislation and institutional requirements. The participants provided their written informed consent to participate in this study.

Author contributions

JT: Methodology, Software, Validation, Writing—original draft. HW: Funding acquisition, Project administration, Writing—review and editing. HL: Investigation, Methodology, Writing—review and editing. YY: Validation, Writing—review and editing. LL: Validation, Writing—review and editing. JN: Funding acquisition, Project administration, Writing—review and editing. BC: Funding acquisition, Project administration, Writing—review and editing.

Funding

The author(s) declare financial support was received for the research, authorship, and/or publication of this article. This research was supported by the Science and Technology (S&T) Program of Hebei under Grant 216Z1803G and the National Key Science and

Technology Project Undertaken by Shenzhen under Grant CJGJZD20220517142405013.

Conflict of interest

The authors declare that the research was conducted in the absence of any commercial or financial relationships that could be construed as a potential conflict of interest.

Publisher's note

All claims expressed in this article are solely those of the authors and do not necessarily represent those of their affiliated organizations, or those of the publisher, the editors and the reviewers. Any product that may be evaluated in this article, or claim that may be made by its manufacturer, is not guaranteed or endorsed by the publisher.

References

- Artz, E. J. (2015). Myoelectric control of a robotic exoskeleton for rehabilitation. *Master's Thesis*. Houston, Texas, USA: Rice University.
- Bernhardt, M., Frey, M., Colombo, G., and Riener, R. (2005). "Hybrid force-position control yields cooperative behaviour of the rehabilitation robot Lokomat," in *9th international Conference on rehabilitation robotics (ICORR)* (Chicago, IL, USA: IEEE), 536–539. doi:10.1109/ICORR.2005.1501159
- Cao, W., Ma, Y., Chen, C., Zhang, J., and Wu, X. (2022). Hardware circuits design and performance evaluation of a soft lower limb exoskeleton. *IEEE Trans. Biomed. Circuits Syst.* 16 (3), 384–394. doi:10.1109/TBCAS.2022.3173965
- Cao, W., Shang, D., Yin, M., Li, X., Xu, T., Zhang, L., et al. (2023). Development and evaluation of a hip exoskeleton for lateral resistance walk exercise. *IEEE/ASME Trans. Mechatronics* 28 (4), 1966–1974. doi:10.1109/TMECH.2023.3273717
- Chiyohara, S., Furukawa, J., Noda, T., Morimoto, J., and Imamizu, H. (2020). Passive training with upper extremity exoskeleton robot affects proprioceptive acuity and performance of motor learning. *Sci. Rep.* 10 (1), 11820. doi:10.1038/s41598-020-68711-x
- Dulyan, L., Talozzi, L., Pacella, V., Corbetta, M., Forkel, S. J., and Thiebaut de Schotten, M. (2022). Longitudinal prediction of motor dysfunction after stroke: a disconnectome study. *Brain Struct. Funct.* 227 (9), 3085–3098. doi:10.1007/s00429-022-02589-5
- Feigin, V. L., Lawes, C. M., Bennett, D. A., Barker-Collo, S. L., and Parag, V. (2009). Worldwide stroke incidence and early case fatality reported in 56 population-based studies: a systematic review. *Lancet Neurology* 8 (4), 355–369. doi:10.1016/S1474-4422(09)70025-0
- Huo, W., Moon, H., Alouane, M. A., Bonnet, V., Huang, J., Amirat, Y., et al. (2022). Impedance modulation control of a lower-limb exoskeleton to assist sit-to-stand movements. *IEEE Trans. Robotics* 38 (2), 1230–1249. doi:10.1109/TRO.2021.3104244
- Ju, M.-S., Lin, C.-C. K., Lin, D.-H., Hwang, I.-S., and Chen, S.-M. (2005). A rehabilitation robot with force-position hybrid fuzzy controller: hybrid fuzzy control of rehabilitation robot. *IEEE Trans. Neural Syst. Rehabilitation Eng.* 13 (3), 349–358. doi:10.1109/TNSRE.2005.847354
- Kawamoto, H., Taal, S., Niniss, H., Hayashi, T., Kamibayashi, K., Eguchi, K., et al. (2010). "Voluntary motion support control of Robot Suit HAL triggered by bioelectrical signal for hemiplegia," in *2010 annual international conference of the IEEE engineering in medicine and biology* (Buenos Aires, Argentina: IEEE), 462–466. doi:10.1109/IEMBS.2010.5626191
- Khoshdel, V., Akbarzadeh, A., Naghavi, N., Sharifnezhad, A., and Souzanchi-Kashani, M. (2018). sEMG-based impedance control for lower-limb rehabilitation robot. *Intell. Serv. Robot.* 11 (1), 97–108. doi:10.1007/s11370-017-0239-4
- Krebs, H. I., Volpe, B. T., Williams, D., Celestino, J., Charles, S. K., Lynch, D., et al. (2007). Robot-aided neurorehabilitation: a robot for wrist rehabilitation. *IEEE Trans. Neural Syst. Rehabilitation Eng.* 15 (3), 327–335. doi:10.1109/TNSRE.2007.903899
- Langhorne, P., Bernhardt, J., and Kwakkel, G. (2011). Stroke rehabilitation. *Lancet* 377 (9778), 1693–1702. doi:10.1016/S0140-6736(11)60325-5
- Lotti, N., Xiloyannis, M., Missiroli, F., Bokranz, C., Chiaradia, D., Frisoli, A., et al. (2022). Myoelectric or force control? A comparative study on a soft arm exosuit. *IEEE Trans. Robotics* 38 (3), 1363–1379. doi:10.1109/TRO.2021.3137748
- Lu, L., Wu, Q., Chen, X., Shao, Z., Chen, B., and Wu, H. (2019). Development of a sEMG-based torque estimation control strategy for a soft elbow exoskeleton. *Robotics Aut. Syst.* 111, 88–98. doi:10.1016/j.robot.2018.10.017
- Lv, X., Han, J., Yang, C., and Cong, D. (2017). "Model reference adaptive impedance control in lower limbs rehabilitation robot," in *2017 IEEE international Conference on Information and automation (ICIA)*. 2017 Macao, China (IEEE), 254–259. doi:10.1109/ICInfA.2017.8078915
- Ma, X., Long, X., Yan, Z., Wang, C., Guo, Z., and Wu, X. (2019). "Real-time active control of a lower limb exoskeleton based on sEMG," in *2019 IEEE/ASME international conference on advanced intelligent mechatronics (AIM)* (IEEE), 589–594. doi:10.1109/AIM.2019.8868817
- Meng, W., Liu, Q., Zhou, Z., Ai, Q., Sheng, B., Xie, S., et al. (2015). Recent development of mechanisms and control strategies for robot-assisted lower limb rehabilitation. *Mechatronics* 31, 132–145. doi:10.1016/j.mechatronics.2015.04.005
- Meng, W., Zhu, Y., Zhou, Z., Chen, K., and Ai, Q. (2014). "Active interaction control of a rehabilitation robot based on motion recognition and adaptive impedance control," in *2014 IEEE international Conference on fuzzy systems (FUZZ-IEEE)* (Beijing, China: IEEE), 1436–1441. doi:10.1109/FUZZ-IEEE.2014.6891705
- Mokhtari, M., Taghizadeh, M., and Mazare, M. (2021). Impedance control based on optimal adaptive high order super twisting sliding mode for a 7-DOF lower limb exoskeleton. *Meccanica* 56, 535–548. doi:10.1007/s11012-021-01308-4
- Navvabi, H., and Markazi, A. H. D. (2019). Hybrid position/force control of Stewart manipulator using extended adaptive fuzzy sliding mode controller (E-AFSMC). *ISA Trans.* 88, 280–295. doi:10.1016/j.isatra.2018.11.037
- Rivas-Blanco, I., Bauzano, E., Cuevas-Rodriguez, M., del Saz-Orozco, P., and Munoz, V. F. (2013). "Force-position control for a miniature camera robotic system for single-site surgery," in *2013 IEEE/RSJ international Conference on intelligent Robots and systems* (Tokyo, Japan: IEEE), 3065–3070. doi:10.1109/IROS.2013.6696790
- Shi, D., Zhang, W., Zhang, W., and Ding, X. (2019). A review on lower limb rehabilitation exoskeleton robots. *Chin. J. Mech. Eng.* 32 (1), 74. doi:10.1186/s10033-019-0389-8
- Shi, Y., Wang, S., Li, J., Gao, X., Lv, J., Lv, P., et al. (2020). "Prediction of continuous motion for lower limb joints based on sEMG signal," in *2020 IEEE international Conference on Mechatronics and automation (ICMA)* (Beijing, China: IEEE), 383–388. doi:10.1109/ICMA49215.2020.9233813
- Singh, R.-J., Chen, S., Ganesh, A., and Hill, M. D. (2018). Long-term neurological, vascular, and mortality outcomes after stroke. *Int. J. Stroke* 13 (8), 787–796. doi:10.1177/1747493018798526
- Sun, P., Shan, R., and Wang, S. (2023). An intelligent rehabilitation robot with passive and active direct switching training: improving intelligence and security of human–robot interaction systems. *IEEE Robotics Automation Mag.* 30 (1), 72–83. doi:10.1109/MRA.2022.3228490

- Taffese, T. B. (2017). *A review of using EEG and EMG psychophysiological measurements in user experience research*. Oulu, Finland: University of Oulu. Master's Thesis.
- Tran, H. T., Cheng, H., Rui, H., Lin, X., Duong, M. K., and Chen, Q. (2016). Evaluation of a fuzzy-based impedance control strategy on a powered lower exoskeleton. *Int. J. Soc. Robotics* 8, 103–123. doi:10.1007/s12369-015-0324-9
- Tsoi, Y. H., Xie, S. Q., and Mallinson, G. D. (2009). "Joint force control of parallel robot for ankle rehabilitation," in *2009 IEEE international Conference on Control and automation* (Christchurch, New Zealand: IEEE), 1856–1861. doi:10.1109/ICCA.2009.5410377
- Valera, A., Díaz-Rodríguez, M., Valles, M., Oliver, E., Mata, V., and Page, A. (2017). Controller–observer design and dynamic parameter identification for model-based control of an electromechanical lower-limb rehabilitation system. *Int. J. Control* 90 (4), 702–714. doi:10.1080/00207179.2016.1215529
- Wang, L., Tian, J., Du, J., Zheng, S., Niu, J., Zhang, Z., et al. (2022). A hybrid mechanism-based robot for end-traction lower limb rehabilitation: design, analysis and experimental evaluation. *Machines* 10 (2), 99. doi:10.3390/machines10020099
- Wu, X., Cao, W., Yu, H., Zhang, Z., Leng, Y., and Zhang, M. (2022). Generating electricity during locomotion modes dominated by negative work via a knee energy-harvesting exoskeleton. *IEEE/ASME Trans. Mechatronics* 27 (6), 4451–4461. doi:10.1109/TMECH.2022.3157848
- Xie, P., Qiu, S., Li, X., Du, Y., Wu, X., and Guo, Z. (2016). "Adaptive trajectory planning of lower limb rehabilitation robot based on EMG and human-robot interaction," in *2016 IEEE international Conference on Information and automation (ICIA)* (Ningbo, China: IEEE), 1273–1277. doi:10.1109/ICInfA.2016.7832015
- Zhang, X., Yue, Z., and Wang, J. (2017). Robotics in lower-limb rehabilitation after stroke. *Behav. Neurol.* 2017, 1–13. doi:10.1155/2017/3731802
- Zhang, Y., Cai, J., Zhang, Y., Ren, T., Zhao, M., and Zhao, Q. (2016). Improvement in stroke-induced motor dysfunction by music-supported therapy: a systematic review and meta-analysis. *Sci. Rep.* 6, 38521. doi:10.1038/srep38521
- Zheng, J., Shi, P., Fan, M., Liang, S., Li, S., and Yu, H. (2021). Effects of passive and active training modes of upper-limb rehabilitation robot on cortical activation: a functional near-infrared spectroscopy study. *NeuroReport* 32 (6), 479–488. doi:10.1097/WNR.0000000000001615
- Zhou, J., Li, Z., Li, X., Wang, X., and Song, R. (2021a). Human–robot cooperation control based on trajectory deformation algorithm for a lower limb rehabilitation robot. *IEEE/ASME Trans. Mechatronics* 26 (6), 3128–3138. doi:10.1109/TMECH.2021.3053562
- Zhou, Y., She, J., Liu, Z.-T., Xu, C., and Yang, Z. (2021b). "Implementation of impedance control for lower-limb rehabilitation robots," in *2021 4th IEEE international Conference on industrial cyber-physical systems (ICPS)* (Victoria, BC, Canada: IEEE), 700–704. doi:10.1109/ICPS49255.2021.9468210